PHYSICAL REVIEW A VOLUME 18, NUMBER 6 DECEMBER 1978

Laser studies of internal conical diffraction. III. Second-harmonic conical refraction in α-iodic acid

A. J. Schell* and N. Bloembergen
Gordon McKay Laboratory, Harvard University, Cambridge, Massachusetts 02138
(Received 10 April 1978)

The phenomenon of nonlinear conical refraction in a noncentrosymmetric biaxial crystal is investigated experimentally. Both free and forced second-harmonic cones are observed, depending on whether the incident laser pulse has wave normals encompassing the optic axis at the second-harmonic or the fundamental frequency, respectively. The photographically recorded second-harmonic intensity patterns at the wavelengths of 0.53 and 0.42 μm are in good agreement with theoretical predictions.

I. INTRODUCTION

This is the third and final paper in a series of laser investigations of intensity patterns in conical refraction. Quantitative intensity distributions for conical refraction were obtained with Gaussian TEM_{00} mode of a helium-neon beam in aragonite[1] and α-iodic acid.[2] The latter crystal is noncentrosymmetric, and if an intense laser input beam is used, second-harmonic radiation is readily observable also in non-phase-matched conditions.

It was predicted nearly a decade ago,[3,4] that the second-harmonic intensity can also show a conical pattern, if the wave normals of the fundamental beam are in the immediate vicinity of an optic axis at the fundamental and/or second-harmonic frequency. A short communication by the present authors of the first experimental demonstration of nonlinear conical refraction was recently published.[5] It is the purpose of this paper to describe more fully the experimental method and results, and also to make a detailed comparison with the theory. The notation and coordinate reference system used will be the same as that adopted in I and II. The optic axis is in the $\hat{v}$ direction, normal to the crystal face which contains the $\hat{y}$ axis, associated with the intermediate principal value $\epsilon_y = n_y^2$ of the dielectric constant. The fundamental laser beam is near normal incidence. The interest is in wave normals $\hat{s}$ nearly parallel to the optic axis. The polar angle between $\hat{s}$ and $\hat{v}$ is θ, the azimuthal angle ϕ is measured from the $\hat{u}$ axis, as indicated in Fig. 1. The incident laser beam is polarized parallel to the $\hat{u}$ axis. It will be shown in Sec. II that the second-harmonic polarization induced in the crystal is then parallel to $\hat{y}$. To satisfy the boundary conditions in the crystal face[6] at the second-harmonic frequency, there will be a free second-harmonic plane wave also polarized in the $\hat{y}$ direction, in addition to the forced polarization wave. The latter is confined to those regions of the crystal in which there is fundamental field intensity. If the wave normals of the incident wave contain the direction of the optic axis at the fundamental frequency, this intensity will be distributed in a conical pattern; i.e., there will be a forced second-harmonic cone. If the dispersion in the direction of the optic axes is sufficiently large, the free harmonic-wave vectors will not contain the direction of the second-harmonic optic axis. Thus the energy associated with the free-wave mode will be refracted in a single spot. This situation is shown in Fig. 2.

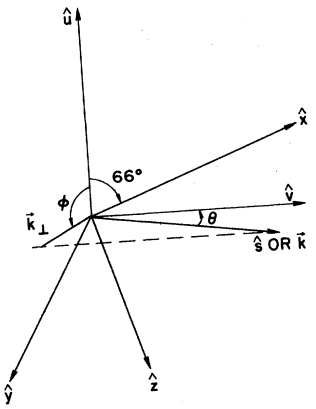

FIG. 1. Geometry of the experiment. $\hat{x}$, $\hat{y}$, $\hat{z}$ are the crystallographic axes of the orthorhombic crystal, α–HIO_3. The optic axis $\hat{v}$ is normal to the entry face. The incident fundamental is polarized in the $\hat{u}$ direction, the second-harmonic polarization is along the $\hat{y}$ axis. The wave normal $\hat{s}$ of all waves makes a small polar angle θ with the optic axis; its azimuthal angle ϕ is measured from the $\hat{u}$ axis.

If the incident laser beam has a bundle of wave normals that contains the second-harmonic optic axis, the free-wave solution gives rise to a free second-harmonic conical intensity pattern. The fundamental intensity is now confined to a single ray, as the fundamental optic axis is not contained in the wave-normal bundle. Consequently, the forced second-harmonic wave gives rise to a

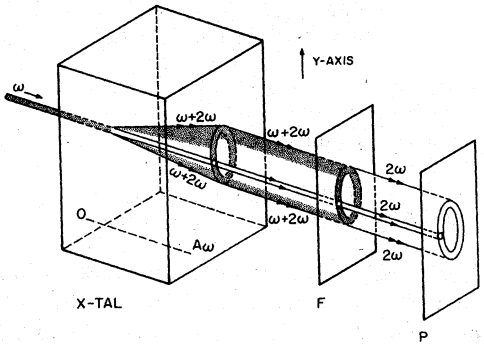

FIG. 2. Forced second-harmonic conical fraction. The fundamental wave vector is parallel to the fundamental optic axis. The free second wave leads to a separate ray direction.

forced ray spot, as shown in Fig. 3.

The apex angle of the cone is given by

$$\tan\rho = \epsilon_y[(\epsilon_x^{-1} - \epsilon_y^{-1})(\epsilon_y^{-1} - \epsilon_z^{-1})]^{1/2}, \tag{1}$$

where $\epsilon_x < \epsilon_y < \epsilon_z$ and where the principal values of ϵ at the fundamental frequency have to be used for the forced cone, and those at the second-harmonic frequency for the free cone.

The condition that indeed a conical pattern with a dark center is observed requires the following condition on the waist w_0 of the incident Gaussian spot and the thickness of the crystal,[1]

$$w^2(L) = w_0^2[1 + (\lambda L/\pi w_0^2 \epsilon_y^{1/2})^2] < (L\rho/2)^2. \tag{2}$$

The additional complications that arise from the presence of natural optical activity, which is always present in biaxial noncentrosymmetric crystals, have been investigated in detail in II. If most of the intensity is associated with polar angles θ satisfying the condition,

$$\tfrac{1}{2}\rho > \theta > 10(\hat{s}\cdot\hat{\Gamma})\epsilon_y/\rho \tag{3}$$

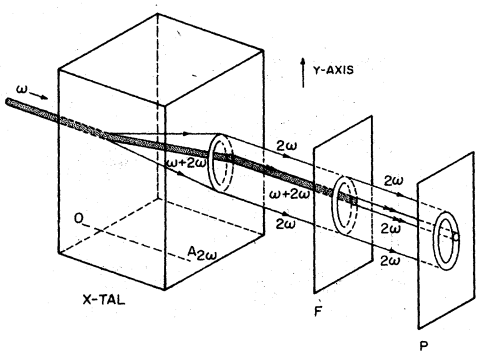

FIG. 3. Free second-harmonic conical refraction. The fundamental wave vector is parallel to the second-harmonic optic axis. The forced second-harmonic wave leads to a ray spot, coinciding with the fundamental ray.

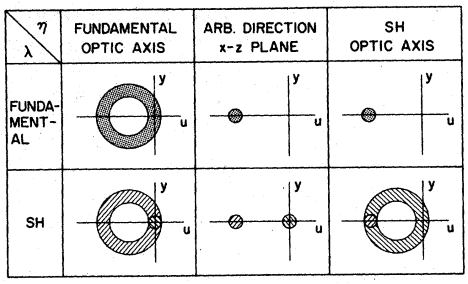

FIG. 4. Schematic intensity distributions at the fundamental and second-harmonic frequency, as a function of the direction of the wave normal of incident fundamental mode, polarized in the $\hat{u}$ direction.

the effects of the rotary power

$$\zeta = \pi\epsilon_y^{3/4}(\hat{s}\cdot\hat{\Gamma})/\lambda_0 \tag{4}$$

may be ignored.[2]

The experimental conditions described in Sec. II are so chosen as to satisfy the geometry in Fig. 1 and the conditions of Eqs. (2) and (3). Photographs of the fundamental and second-harmonic intensity patterns for a range of angles in the vicinity of the optic axes are presented in Sec. II.

A more detailed theoretical discussion is given in Sec. III. It is shown that the general case of second-harmonic generation in biaxial crystals is considerably more complex than the special geometry discussed in this Introduction. Quantitative theoretical considerations, applied to the experimental geometry, confirm the rather qualitative and intuitive arguments given in this Introduction. These are summarized in Fig. 4.

II. EXPERIMENTAL METHOD AND RESULTS

A. Properties of α-iodic acid

α-iodic acid was suggested in the first publication on nonlinear conical refraction.[3] It has a rather large cone angle 2ρ and can be grown in crystals of good optical quality with linear dimensions of several cm. Thus the condition of Eq. (2) is readily satisfied. Furthermore, α-iodic acid has a rather large nonlinear susceptibility, and second-harmonic generation is readily observable even in non-phasematched conditions.[7] The crystal has orthorhombic symmetry D_2, so that the principal axes of the dielectric tensor coincide with the crystallographic axes. This greatly facilitates the alignment procedures. The crystal is soft, and optical polishing of the faces is rather difficult. Some waviness of the surface remained, but it is of no consequence for the experiments in this paper. The crystal used in these experiments had faces perpendicular (within a few degrees) to the optic axis and had a thickness $L = 2.4$ cm.

TABLE I. Measured values of d_{14} in α-HIO_3 relative to other nonlinear coefficients.

$\lambda(\mu m)$	$LiNbO_3$ (d_{31})	KDP (d_{36})	$LiIO_3$ (d_{33})	α-SiO_2 (d_{11})	Reference
1.06	•••	13.1 ± 1	1.08 ± 0.1	16.1 ± 0.5	Crane (Ref. 10)
1.065	1.5 ± 0.5	•••	•••	20 ± 5	Kurtz (Ref. 7)
1.15	•••	10	•••	•••	Bjorkholm (Ref. 9a)

Further details about sample preparation may be found in II.

The index of refraction data, measured by Kurtz *et al.*,[7] are listed in Table I. From these one computes the angle between the optic axis and the z axis.

$$\eta = \arctan[(\epsilon_x^{-1} - \epsilon_y^{-1})/(\epsilon_y^{-1} - \epsilon_z^{-1})]^{1/2}. \quad (5)$$

The variation of η with frequency is related to the dispersion of the indices by

$$\Delta\eta = \frac{1}{2}\left(\frac{n_x - n_y}{n_y - n_z}\right)^{1/2}\left(\frac{\Delta n_z}{n_x - n_z} + \frac{\Delta n_y}{n_x - n_y} + \frac{(n_y - n_z)\Delta n_x}{(n_x - n_z)(n_x - n_y)}\right). \quad (6)$$

If the index of refraction measurements are good to 0.0001, then

$$\Delta\eta \leq 0.1°.$$

This does not account for the large scatter in the calculated values (shown as dots in Fig. 5). In the originally proposed experiment which relied on the calculated dispersion, the 1.06-μm optic axis was expected to be 0.008 rad from the second-harmonic optic axis. This separation was found to be less than 0.002 rad. Since the dispersion of the optic axes is very important in the interpretation of the nonlinear conical refraction results, it was decided to measure the dispersion of the optic axis directly by a conoscopic method. This procedure also serves to align the crystal accurately.

Since each principal dielectric axis coincides with the same crystallographic axis throughout the range 2ω to ω, the optic axes of this frequency range lie in the same crystallographic plane, the optical x-z plane. The alignment was performed by using colinear beams of an argon-ion laser at 454.5 nm and a helium-neon laser at 632.8 nm, as shown in Fig. 6. A lens with focal length of 100 cm was used to focus the light beams on the face of the crystal. The crystal was mounted on the u state of a Leitz four-axis universal stage, and adjusted with the inner degrees of freedom of tilt and rotation so that the outermost axis was parallel to the y axis. This could be verified by observing conical patterns at the red and blue wavelength, respectively, by turning the crystal 1.3° about the y axis. After the crystal has been so oriented, the dispersion of the optic axes was measured at a number of other laser frequencies giving rise to the square points in Fig. 5.

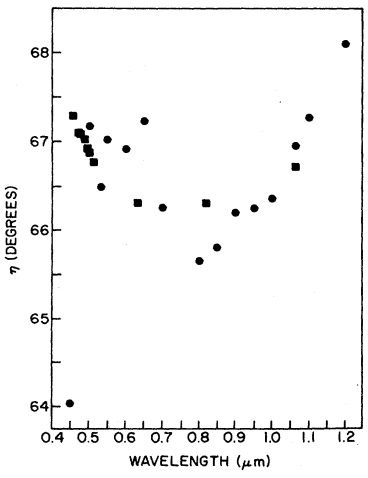

FIG. 5. Dispersion of the optic axis in α-HIO_3, which makes an angle η with the crystallographic $\hat{z}$ axis. Solid squares are our experimental data; solid circles are calculated from indices of refraction.

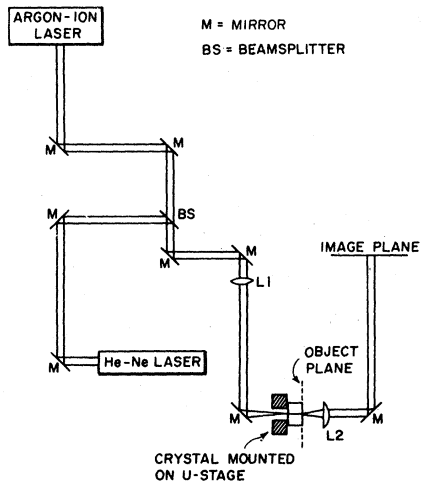

FIG. 6. Experimental arrangement to align the biaxial orthorhombic crystal.

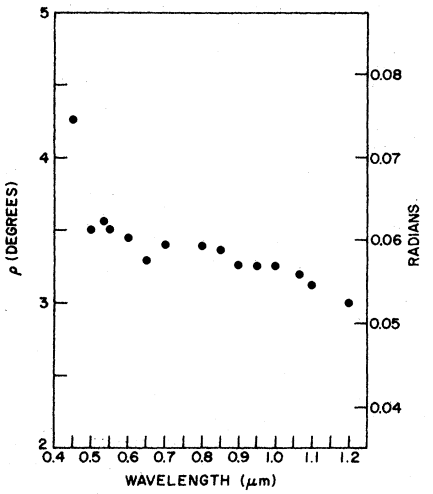

FIG. 7. Apex cone angle in α-iodic acid as a function of wavelength, computed from index of refraction data.

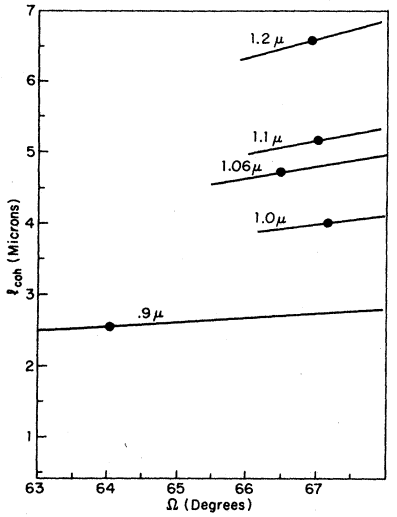

FIG. 8. Second-harmonic coherence length, at various wavelengths, for small variations in direction near the optic axis in α-HIO_3. Ω is the angle with respect to the crystal's z axis. The solid circles mark the values at the SH optic axis.

The cone angle, given by Eq. (1), is about 3.5° at 500 nm and decreases to 3° in the near infrared. The data computed from the index of refraction are shown in Fig. 7.

The nonlinear susceptibility elements $\chi^{(3)}$ are only nonvanishing if all three Cartesian indices are different, in the orthorhombic D_2 symmetry which has three orthogonal two fold axes (2, 2, 2). For second-harmonic generation in α-iodic acid, one has three independent coefficients.

$$d_{14}=\chi_{xyz}(-2\omega,\omega,\omega)=\chi_{xzy}(-2\omega,\omega,\omega),$$

$$d_{25}=\chi_{yxz}(-2\omega,\omega,\omega)=\chi_{yzx}(-2\omega,\omega,\omega),$$

$$d_{36}=\chi_{zxy}(-2\omega,\omega,\omega)=\chi_{zyx}(-2\omega,\omega,\omega).$$

The difference between these three coefficients, due to nonlinear dispersion, is rather small and may be ignored for our purposes. This leads to the Kleinman symmetry condition[8] $d_{14}=d_{25}=d_{36}$. This nonlinear coefficient has been measured by various authors[7,9-11] relative to quartz, KDP and $LiIO_3$, as shown in Table I. The absolute value which results is

$$d_{14}(\alpha\text{-}HIO_3)=4\times10^{-8}\ \text{cm/statvolt}.$$

For an input field linearly polarized along the $\hat{u}$ axis as described in Fig. 1, the fundamental field components inside the crystal are

$$E_x=\tfrac{1}{2}E_0\exp(ik_v r-i\omega t)\sin\eta+\text{c. c.},$$

$$E_z=\tfrac{1}{2}E_0\exp(ik_v r-i\omega t)\cos\eta+\text{c. c.}.$$

The second-harmonic polarization is in the y direction

$$P_y(2\omega)=2d_{25}E_x(\omega)E_z(\omega). \tag{7}$$

Since the wave normals are required to lie in the vicinity of the optic axis, it would be fortuitous, if a phase-matching condition were satisfied. The coherence length is given by

$$l_{coh}=\frac{\pi c}{2\omega}\frac{1}{n_y(2\omega)-n_y(\omega)}=\frac{\pi}{\Delta k} \tag{8}$$

as the index of refraction for light propagating near the optic axis is the same for the $\hat{u}$ and $\hat{y}$ direction. The coherence length is indeed short, less than 5 μm, and is plotted for different fundamental wavelengths in Fig. 8. The variation with angular orientation is negligible in the range of interest.

The second-harmonic power in the separated free and forced second-harmonic beams is

$$\mathcal{P}(2\omega)=\frac{128\pi^5\omega^2(2d_{25})^2\mathcal{P}^2(\omega)\sin^2\eta\cos^2\eta}{c^5w_0^2(\Delta k)^2n^4(\omega)n^2(2\omega)}, \tag{9}$$

where the power in the fundamental Gaussian beam of waist w_0 is

$$\mathcal{P}(\omega)=(c/8\pi)\,|E_0|^2w_0^2n_w. \tag{10}$$

As will be discussed more fully in Sec. III, the free and forced waves, with wave vectors normal to the crystal, do not give rise to Maker interference fringes,[12] because the Poynting vectors in the geometry of interest are sufficiently different so that no overlap between the free and forced intensity is present at the exit surface.

B. Experimental method

The second-harmonic power generation was first observed with the input pulse of a Nd-glass laser. Sufficient green light was readily detectable in the unfocused beam. In practice the laser beam was focused to a waist size $w_0 = 50-60$ μm on the entrance face. In this case both Eqs. (2) and (3) are satisfied. Thus the effect of natural activity may be ignored, as the modes are nearly linearly polarized.

The far-field diffraction angle for this spot size is about 0.2°. This is small compared to the cone angle of 3.5°, but large enough so that the intensity pattern did not become unduly sensitive to crystal orientation, which was reproducible to 0.1°. The finer details of conical refraction in a crystal with optical activity were investigated in II, but the effects of rotary power are not of interest in establishing the main characteristics of nonlinear conical refraction. For a spot size of 60 μm, most of the intensity is associated with angles θ, satisfying the inequality of Eq. (3). The eigenmodes may the be considered to have constant linear polarization.

The Nd-glass laser was of a conventional type, passively Q-switched.[13] The beam profile was measured with a photo diode array. Diffraction limited operation was obtained for a TEM_{00} mode with a waist of 600 μm, in 0.03-J pulses for 120 $\times 10^{-9}$ sec duration. The repetition rate was 3 pulses per minute. The beam was focused with a 20-cm focal length on the crystal, giving a spot size of 60 μm on the crystal. As the data in Fig. 5 show, the optic axes at 1.06 and 0.53 μm make an angle of less than 0.1°. This unfortunate circumstance implies that, contrary to earlier estimates, the conditions of Figs. 2 and 3 for distinguishable free and forced second-harmonic cones could not be met at this wavelength.

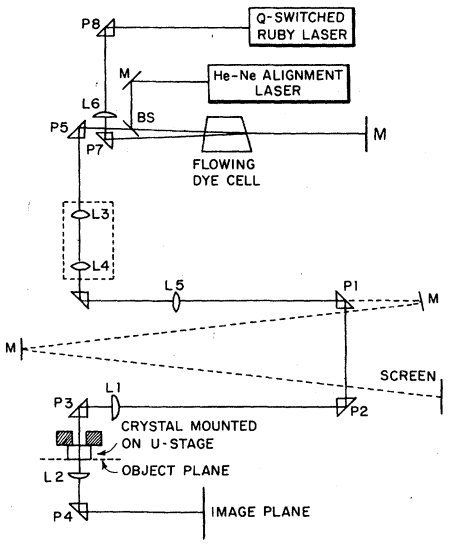

FIG. 9. Experimental arrangement to observe second-harmonic conical refraction at 0.41 μm.

Most of the final data were therefore taken with a fundamental wavelength at 0.82 μm. The second harmonic at 0.41 μm is just below the ultraviolet absorption edge of the crystal. Advantage is taken of the large ultraviolet dispersion, and the angle between the optic axes at the fundamental and second-harmonic frequency is now 1.8°.

The fundamental pulse is derived from a ruby pumped dye laser, described by Kramer.[14] Figure 9 shows the diagram of the experimental apparatus. A dielectric mirror with a reflectivity $>90\%$ between 0.81 and 0.84 μm was used as a rear reflector. The dye used was 1, 1′, 3, 3, 3′, 3′-hexamethyl-indotricarbocyanine iodide[15] (Eastman Kodak No. 14086) in reagent grade dimethyl sulfoxide. Because the dye laser was 6 m from the crystal mount, a telescope reduced the beam diameter by a factor of 4. Large focal length lenses, 20 and 5.0 cm, were used to avoid large aberrations. A Schott RG-780 filter absorbed extraneous light from the laser. The dashed line shows the path of the He-Ne alignment laser and the dye laser beams when the prism $P1$ was removed to check their colinearity. The dye laser beam's divergence after lens $L5$ was 0.7 mrad. The radius of the dye laser beam at lens $L1$ was 1 mm; the full angular width of the focused beam in the crystal was 0.4°. The estimated radius of the focal spot was 60 μm. The laser bandwidth had to be narrow enough so that the fundamental and second-harmonic conical refraction patterns were blurred over an angular range much smaller than the angular spread of the focused beam in the crystal. As seen in Fig. 5, the 90-Å bandwidth causes an optic axis spread of about 0.1° which is negligible.

The exit plane of the crystal was imaged by the lens $L2$ onto a photographic plate, with a magnification of 8. The fundamental intensity patterns were recorded on hypersensitized Eastman Kodak Type (I-Z) spectroscopic plates. Immediate development after exposure reduced background fog. A single shot produced sufficient exposure.

The second-harmonic intensity is roughly 10^6 times smaller. The second-harmonic photographs were taken on Eastman Kodak Royal-X 4× 5 in. sheet film and tray developed in HC-110 (dilution A) for 7 min, which gave an effective ASA of 4000. In such exposures the fundamental light was filtered out with a Schott BG-18 filter.

It so happens, however, that Royal-X, an orthochromatic film, has such a low sensitivity at 1.06 μm as to provide a natural compensation for the

large difference between fundamental and second-harmonic intensity. Thus the second-harmonic and fundamental patterns could be simultaneously photographed without filters. When the same technique of superposition of fundamental and second-harmonic patterns was used at 0.82 and 0.41 μm respectively, the 0.82 fundamental pattern was overexposed. However, it did not obscure the second-harmonic pattern, and the overexposure could be corrected by an appropriate filter. The Royal-X exposures of the 0.53 μm were made with 200–1000 laser shots; the 0.41-μm exposures were made with 800–3000 laser shots. Polaroid high-speed recording film Type 410 was also used in some of the exposures.

C. Experimental intensity patterns

Figure 10 shows the observed intensity patterns at ω and 2ω for the 0.82-μm fundamental as the angle between the laser wave vector and the 0.82-μm optic axis is varied. The photographs in the top row are the fundamental patterns; in the middle row, the superposition of the fundamental and second-harmonic (SH) patterns; and in the third row, the patterns of the SH alone.

When the laser beam coincides with neither optic axis, nonlinear birefringence is observed. Because the laser beam was not completely polarized perpendicular to the y axis, there is an extra spot seen in the middle row of the 1.5° column. This is the other birefringent beam of the fundamental which is sufficiently weak so that it only appears in a time exposure.

When the laser beam coincides with the SH optic axis, the free wave is conically refracted as is shown in the last columns of Fig. 10. The diameter of the conical refraction circle appears larger at 0.41 μm than at 0.82 μm; this is in qualitative agreement with Fig. 7. The observed SH pattern is complicated by the effects of natural optical activity. The laser beam has components polarized parallel and perpendicular to the y axis, due to the optical rotation in the crystal, but the SH source polarization is still given by Eq. (7) because the two fundamental beams are spatially separated at the exit surface of the crystal and because a purely y polarized beam cannot generate SH-source polarization in α-HIO_3. Therefore, only one forced SH spot should be observed even for unpolarized laser light. The SH intensity pattern has two spots, one of which corresponds to the fundamental y axis. The other spot is anomalous and does not appear in the superposition photograph. It is probably caused by a spurious change in orientation of the crystal between exposures.

When the laser beam coincides with the fundamental optic axis, conical refraction of the forced wave is observed, as is shown in the first and second columns of Fig. 10. The forced ring and the free spot were predicted in the Introduction (compare Fig. 2).

For orientations containing neither optic axis, a forced and a free second-harmonic ray spot are seen. Thus the patterns are at least in qualitative agreement with the expectations of the Introduction, shown in Fig. 4.

The intensity patterns produced by the 1.06-μm fundamental are shown in Fig. 11 as a function of the angle of the laser beam with respect to the fundamental optic axis. The optic axes at 1.06 and 0.53 μm are very nearly colinear, and a superposition of forced and free ring patterns, which was predicted by Shih and Bloembergen,[4] is ob-

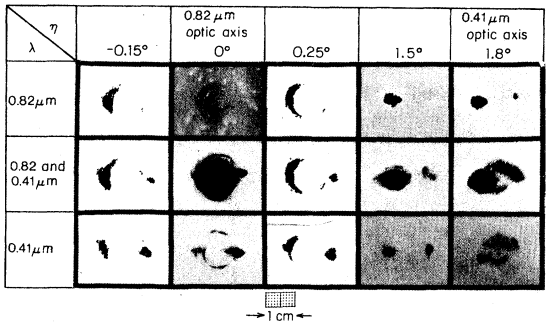

FIG. 10. Observed intensity patterns at the exit surface of a 2.4-cm thick crystal of α-iodic acid (magnification 8×). The angle between the light wave vectors and the optical axis at the fundamental wavelength (0.82 μm) is varied as indicated. The total power at the second harmonic is about one millionth of the fundamental power.

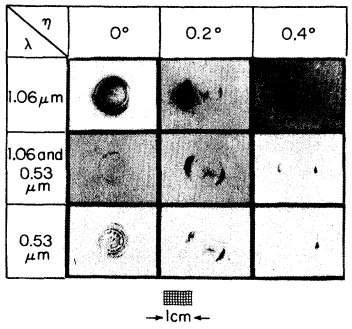

FIG. 11. Intensity patterns at 1.06 and 0.53 μm as a function of the angle between the wave normal and the fundamental optic axis. The SH optic axis is in nearly the same direction.

served when the laser beam is directed along the coincident optic axes. The good mode quality of the Nd-glass laser produces a well-collimated free SH wave which is diffracted in the same manner as the incident y-polarized beam shown in Fig. 5(b) of II. Parts of the forced ring are present, but the total intensity is much less than that of the free wave. This is because the fundamental beam with an intensity $I(0)$ at the entrance surface of the crystal has at the exit surface of the crystal an intensity $I(L)$ which is roughly

$$I(L) = \theta I(0)/4A \cong I(0)/10.$$

The intensity of free SH wave is

$$I^{\text{free}}(L) \propto \theta(I(0))^2/4A$$

while the intensity of forced SH wave is

$$I^{\text{forced}}(L) \propto [\theta I(0)/4A]^2.$$

Therefore,

$$I^{\text{forced}}(L)/I^{\text{free}}(L) \cong 1/10.$$

The relative intensities of the forced and the free waves are accentuated by the high-contrast Royal-X film.

Figures 10 and 11 show all of the essential predicted features of nonlinear conical refraction. The experimental intensity patterns are not nearly as precise as those obtained for linear conical refraction (described in II), due to imperfections in the crystal, uncalibrated photography, and, in the case of the 0.82-μm fundamental, poor mode quality of the laser beam. Further comparison with theory will be postponed to Sec. III, where more detailed theoretical considerations will be presented.

III. THEORETICAL DISCUSSION OF NONLINEAR CONICAL REFRACTION

A. Forced and free harmonic waves in a biaxial crystal

When an unpolarized light beam is incident at an arbitrary angle and polarization, birefringence leads, in general, to two diffracted wave vectors in the crystal, $k_{1F} = (\omega/c)n_{1F}\hat{s}_{1F}$ and $k_{2F} = (\omega/c)n_{2F}\hat{s}_{2F}$, each with a well-defined linear polarization. The induced second-harmonic polarization will, in general, consist of three components with three different wave vectors, shown in Fig. 12. If the incident and transmitted laser beams have finite cross sections, the harmonic-source polarization is confined to the regions where beam intensities are present. The polarization $P^{11}(2\omega)$ with wave vector $2\vec{k}_{1F}$ is confined to the region of ray 1. Similarly, the polarization $P^{22}(2\omega)$ is confined to the region of ray 2. The cross polarization $P^{12}(2\omega)$ is confined to the region of overlap between the two rays, as indicated in Fig. 13. The wave-vector directions have tangential components equal to, or twice, the tangential component of the incident wave vector. If the incident wave vector is normal, all wave vectors are normal to the entrance surface, but the Poynting vectors will still have different degrees of walk-off, as shown in Fig. 13.

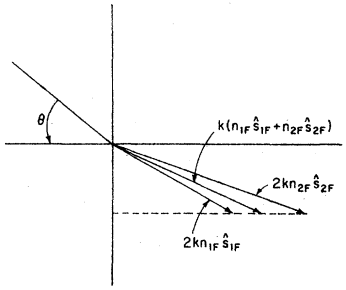

FIG. 12. Three wave vectors of second-harmonic polarization.

Second-harmonic polarization in each of the three wave-vector modes has its own direction and magnitude,

$$P_i^m(2\omega) = \chi_{ijk}^{(3)}(-2\omega, \omega, \omega)E_j^m(\omega)E_k^n, \tag{11}$$

where $m,n = 1, 2$ and ijk denote Cartesian coordinates.

Select one of the three harmonic polarization sources and drop the indices 1, 2.

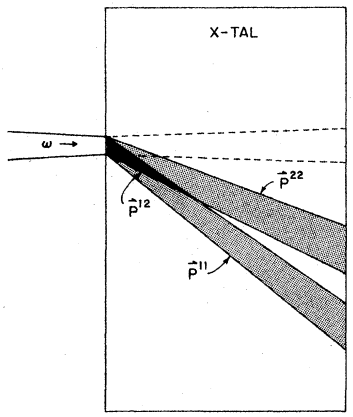

FIG. 13. Spatial distribution of the second-harmonic polarization with different wave vectors produced by a single incident fundamental ray.

$$\vec{P}^{NLS}(2\omega) = P_0 \hat{p} \exp[i(2\omega/c) n_F (\hat{s}\cdot\vec{r})]. \quad (12)$$

The SH electric field created by this source term obeys the wave equation

$$\vec{\nabla}\times(\vec{\nabla}\times\vec{E}) - \vec{\epsilon}(2\omega)(2\omega/c)^2\vec{E} = 4\pi(2\omega/c)^2\vec{P}^{NLS} \quad (13)$$

The solution of this inhomogeneous equation in an anisotropic crystal was discussed by Kleinman[8] and Pershan.[16] A particular solution, the forced second-harmonic wave, is given by

$$E^{inh} = (A_1\hat{e}_1 + A_2\hat{e}_2 + A_3\hat{e}_3) \exp[i(2\omega/c) n_F (\hat{s}\cdot\vec{r})]. \quad (14)$$

Here $\hat{e}_1$ and $\hat{e}_2$ are the directions of the electric field of the two modes at 2ω with wave-vector directions $\hat{s}$. They are related by the dielectric tensor to the unit directions of the displacement vector $\hat{d}_1$ and $\hat{d}_2$, which are normal to $\hat{s}$. Note that $\hat{e}_\nu$ and $\hat{d}_\nu$ ($\nu = 1, 2$) are defined by $\hat{s}$. Kleinman and Pershan have shown that

$$A_\nu = \frac{4\pi P_0 \exp[i(2\omega/c) n_F (\hat{s}\cdot\vec{r})]}{(n_F^2 - n_{\nu,s}^2)(\hat{d}_\nu\cdot\hat{e}_\nu)} \times \left(\hat{d}_\nu\cdot\hat{p} - \frac{(\hat{d}_\nu\cdot\vec{\epsilon}\cdot\hat{s})(\hat{p}\cdot\hat{s})}{\epsilon}\right). \quad (15)$$

Here $n_{\nu,s}$ ($\nu = 1, 2$) are the two effective refractive indices at 2ω associated with the wave normal $\hat{s}$. The third component of the electric field, orthogonal to $\hat{e}_1$ and $\hat{e}_2$, is approximately

$$A_3 = -4\pi P_0 (\hat{p}\cdot\hat{e}_3)/\epsilon . \quad (16)$$

In general, two solutions of the homogeneous wave equation with amplitudes A_1 and A_2 and polarization directions $\hat{e}_1$ and $\hat{e}_2$, must be added to the inhomogeneous forced wave solution to satisfy the boundary conditions. If we ignore the small reflected harmonic amplitudes, the boundary condition is simply that the tangential components of $E(2\omega)$ must vanish. The total second-harmonic field is consequently, if $\hat{e}_3$ is normal to the boundary,

$$\vec{E}(2\omega) = A_1\hat{e}_1\{\exp[i(2\omega/c) n_F (\hat{s}\cdot\vec{r})] - \exp[i(2\omega/c) n_{1\hat{s}} (\hat{s}\cdot\vec{r})]\} + A_2\hat{e}_2\{\exp[i(2\omega/c) n_F (\hat{s}\cdot\vec{r})] - \exp[i(2\omega/c) n_{2\hat{s}} (\hat{s}\cdot\vec{r})]\} + A_3\hat{e}_3 \exp[i(2\omega/c) n_F (\hat{s}\cdot\vec{r})]. \quad (17)$$

For each of the three source polarization wave vectors a solution given by Eqs. (15)–(17) exists.

Considerable simplification can be obtained by a judicious choice of the incident polarization. In the experiments described in this paper, one has

$$\hat{p}\cdot\hat{d}_1 = 1, \quad \hat{p}\cdot\hat{s} = \hat{p}\cdot\hat{e}_3 = 0, \quad \hat{p}\cdot\hat{d}_2 = 0,$$

where $\hat{d}_1$ is in the $\hat{y}$ direction. Thus the SH electric field becomes simply

$$\vec{E}(2\omega) = \hat{y}\,\frac{4\pi\omega}{nc\Delta k} P_0\{\exp[i(2\omega/c) n_F (\hat{s}\cdot\vec{r})] - \exp[i(2\omega/c) n_y(2\omega)(\hat{s}\cdot\vec{r})]\}, \quad (18)$$

where the forced and free plane waves overlap, they give rise to the well known interference fringes. Second-harmonic conical refraction is, of course, essentially connected with the walk off of the Poynting vectors for beams of finite diameter.[17,18] If the difference in optic axes is appreciable, the experimental conditions are such that the rays associated with the free and forced solutions do not overlap at the exit surface of the crystal. Equation (18) shows that the total power associated with the separated forced wave is the same as that associated with the free wave.

The detailed solution for a (Gaussian) beam of finite diameter can be obtained from the homogeneous plane-wave solution, by a two-dimensional Fourier decomposition of the incident field, corresponding to a distribution of direction or transverse wave-vector components. This procedure was developed by Kleinman *et al.*[17,18] to discuss harmonic generation by Gaussian beams in anisotropic crystals, and it was used by Shih and Bloembergen[4] to calculate SH conical refraction. They assumed that the fundamental beam is well collimated, and everywhere parallel to the fundamental optic axis. This assumption requires that the crystal length satisfies the inequality

$$L \ll n_y \pi w_0^2/\lambda. \quad (19)$$

This requirement means that the fundamental and SH wave vectors to first order in θ will give the phase at the exit surface of the crystal to a small fraction of π. When the fundamental beam is directed along the SH optic axis and polarized perpendicular to the y axis, the SH electric field at the exit surface is given by

$$\vec{E}(u,y,L)=\frac{2\omega}{cn_{2\omega}}\int d^2K_\perp P(K_\perp)\exp(i\vec{K}_\perp\cdot\vec{r}_\perp)$$
$$\times\left(\frac{\hat{e}_1\cos\tfrac{1}{2}\phi(\exp(iK_vL)-\exp\{i[k_2-AK_\perp(-\cos\phi+1)]L\})}{\Delta k+AK_\perp(-\cos\phi+1)}\right.$$
$$\left.+\frac{\hat{e}_2\sin\tfrac{1}{2}\phi(\exp(iK_vL)-\exp\{i[k_2-AK_\perp(-\cos\phi-1)]L\})}{\Delta k+AK_\perp(-\cos\phi-1)}\right), \tag{20}$$

where K_v is twice the component of the fundamental wave vector directed along the optic axis, and

$$k_2=(2\omega/c)n_{2\omega}, \tag{21a}$$
$$(K_\perp)_u=k_2\theta\cos\phi, \tag{21b}$$
$$(K_\perp)_y=k_2\theta\sin\phi, \tag{21c}$$
$$\hat{e}_1=-\sin\tfrac{1}{2}\phi\hat{u}+\cos\tfrac{1}{2}\phi\hat{y}, \tag{21d}$$
$$\hat{e}_2=\cos\tfrac{1}{2}\phi\hat{u}+\sin\tfrac{1}{2}\phi\hat{y}. \tag{21e}$$

$P(k_u, k_y)$ is the Fourier transform of the transverse spatial distribution of second-harmonic polarization,

$$P(\vec{K}_\perp)=\frac{1}{2\pi}\exp(-iK_vL)\int P(\vec{r}_\perp)\exp(i\vec{K}_\perp\cdot\vec{r}_\perp)\,d^2r_\perp. \tag{22}$$

Equation (20) may be simplified if

$$\Delta k\gg AK_\perp \quad\text{or if}\quad l_{\text{coh}}\ll\pi w_0/\rho.$$

This inequality is amply satisfied for α-HIO_3, with the data given in Sec. II. Equation (20) thus reduces to

$$E(u,y,L)=\frac{4\pi\omega}{n_{2\omega}c\Delta k}P(u,y,L)\hat{y}$$
$$-\frac{2\omega}{n_{2\omega}c}\int d^2K_\perp\,\frac{P(\vec{K}_\perp)}{\Delta k}\exp(i\vec{K}_\perp\cdot\vec{r}_\perp)$$
$$\times(\hat{e}_1\cos\tfrac{1}{2}\phi\exp\{i[k_2-AK_\perp(-\cos\phi+1)]L\}+\hat{e}_2\sin\tfrac{1}{2}\phi\exp\{i[k_2-AK_\perp(-\cos\phi-1)]L\}). \tag{23}$$

With K_v and k_2 constant, Eqs. (22) and (23) describe the SH electric fields only if the near-field condition [Eq. (19)] holds. The validity of Eq. (22) may be extended to the far field if one allows for a dependence of the longitudinal phase factors on the transverse direction, and writes

$$K_v=K_v(\vec{K}_\perp) \quad\text{and}\quad k_2=k_2(\vec{K}_\perp).$$

The integral may be evaluated by the method of stationary phase, which does not require the phase to be accurately known in order to yield useful information, or by numerical integration, provided the wave vectors are calculated exactly rather than to only first order. These procedures have been discussed[2] in detail for linear conical refraction patterns in I and II. The amplitude part of the integrand is zero order in θ, but this is sufficiently accurate.

Equation (23) shows explicitly that the forced SH electric fields are spatially confined to the regions of SH-source polarization regardless of the stationary points of the phase of the forced wave. This is true in the near as well as the far field. Equation (23) may be considered as a Fourier integral superposition of Eq. (18).

The free or homogeneous wave-normal bundles in Eqs. (18) and (23) have the same Poynting vectors as the free solutions discussed in II. When the free wave-vector bundle is directed along the SH optic axis, the corresponding Poynting vectors lie on a cone. The intensity distribution in the ring pattern will depend on $\vec{P}^{\text{NLS}}$. When the free wave-vector bundle does not contain the optic axis at the second-harmonic frequency, the Poynting vectors will define two rays for arbitrary polarization.

Application of Eq. (23) for the specific geometry used in our experiments yields the following results. Since the fundamental field has a wave-vector and electric field direction in the $\hat{x}\hat{z}$ or $\hat{u}\hat{v}$ plane ($\phi=\pi$ or 0), the fundamental field has only one polarization mode.

Far from the optic axes, the fundamental field will have single ray direction, and so does the

second-harmonic forced polarization wave. Since the harmonic polarization is in the $\hat{y}$ direction, the free second-harmonic wave will also be polarized in this direction, and there is consequently only one free mode. The situation depicted in the middle column of Fig. 4 thus results, with two SH ray spots of equal intensity.

When the fundamental wave vector is near the SH, but not near the fundamental optic axis, the situation of Fig. 3 or the last column of Fig. 4 prevails. The free wave intensity pattern is identical to that which would have been obtained in linear conical refraction, if a low intensity light beam at 2ω, polarized in the $\hat{y}$ direction, had been incident on the crystal. The details of this conical refraction pattern have been discussed in II. They are more readily observed and verified in linear experiments described there. The dominant feature is that the "free" part of the SH intensity is distributed in a cone. The "forced" part is still a single ray, coinciding with the one fundamental ray direction.

When the fundamental wave-vector bundle contains the direction of the fundamental optic axis, the field distribution at the fundamental frequency can again be calculated in detail by the methods of II. The polarization associated with wave-vector components in the immediate vicinity of the optic axis will be rotated by natural optical activity. A very small fraction of fundamental intensity is so affected, as rotary power ζ at infrared frequencies is small.[2] Most of the fundamental intensity is associated with wave-vector directions satisfying Eq. (3). The polarization for these components remains linearly polarized, and their intensity is spread into a conical pattern. They produce a second-harmonic polarization in the $\hat{y}$ direction, confined to the same conical mantle as the fundamental intensity. The free second-harmonic wave is also polarized in the $\hat{y}$ direction and gives rise to a single second-harmonic free spot. Thus Eq. (23) reproduces the situation sketched in Fig. 2 and the first column of Fig. 4 in this geometry.

The theory of second-harmonic conical refraction is in essential agreement with the experimental observations, shown in Fig. 10. The experimental patterns are not nearly as precise as those obtained for linear conical refraction described in I and II. It is not possible to obtain intensity distribution with the same precision due to uncalibrated photography, crystal imperfections, and poorer mode quality of the incident high-power laser pulses, especially at the 0.82-μm fundamental wavelength. In principle, Eq. (23) could be evaluated with the same precision as in the linear case. Because the data is only semiquantitative, a satisfactory semiquantitative comparison with the theory requires the calculation of the expected two-dimensional SH intensity pattern. This requires the detailed calculation of the two-dimensional fundamental field pattern, and thus the square of the computing time required for the one-dimensional intensity profiles shown in II. The same degree of quantitative agreement is simply not obtainable in the nonlinear case. The experimental demonstration of the essential features of the theory must suffice.

Although the discussion has been limited to second-harmonic generation, it is clear that similar arguments would apply to other nonlinear processes of parametric generation.

ACKNOWLEDGMENT

This work was carried out in partial fulfillment of the requirements for the Ph.D. degree at Harvard University, and supported by the Joint Services Electronics Program under Contract No. N00014-75-C-0648.

---

*Present address: IBM Thomas J. Watson Research Center, Yorktown Heights, N. Y. 10598.

[1]A. J. Schell and N. Bloembergen, J. Opt. Soc. Am. 68, 1093 (1978). This paper will henceforth be referred to as I.

[2]A. J. Schell and N. Bloembergen, J. Opt. Soc. Am. 68, 1098 (1978). This paper will henceforth be referred to as II.

[3]N. Bloembergen and H. Shih, Opt. Commun. 1, 70 (1969).

[4]H. Shih and N. Bloembergen, Phys. Rev. 184, 895 (1969).

[5]A. J. Schell and N. Bloembergen, Opt. Commun. 21, 150 (1977).

[6]N. Bloembergen and P. S. Pershan, Phys. Rev. 128, 606 (1962).

[7]S.K. Kurtz, T. T. Perry, and J. G. Bergman, Jr., Appl. Phys. Lett. 12, 186 (1968).

[8]D. A. Kleinman, Phys. Rev. 128, 1761 (1962).

[9](a) J. E. Bjorkholm, IEEE J. Quantum Electron. QE-4, 970 (1968); (b) QE-5, 260 (1969).

[10]G. R. Crane, J. Chem. Phys. 62, 3571 (1975).

[11]R. Bechmann and S. K. Kurtz, in *Landolt-Bornstein*, Vol. 2, edited by K. H. Hellwege (Springer, New York, 1969).

[12]P. D. Maker, R. W. Terhune, M. Nisenoff, and C. M. Savage, Phys. Rev. Lett. 8, 21 (1962).

[13]More detailed information may be found in the following theses: W. K. Burns, Ph.D. thesis (Harvard University, 1971) (unpublished); A. J. Schell, Ph.D. thesis (Harvard University, 1977) (unpublished).

[14]S. D. Kramer, Ph.D. thesis (Harvard University, 1976) (unpublished).
[15]Yasushi Miyazoe and Mitsuo Maeda, Appl. Phys. Lett. 12, 206 (1968).
[16]P. S. Pershan, in *Progress in Optics*, Vol. 5, edited by E. Wolf (North-Holland, Amsterdam, 1966), p. 83.
[17]G. D. Boyd, A. Askin, J. M. Dziedzic, and D. A. Kleinman, Phys. Rev. 137, A1305 (1965).
[18]D. A. Kleinman, A. Askin, and G. D. Boyd, Phys. Rev. 145, 338 (1966).

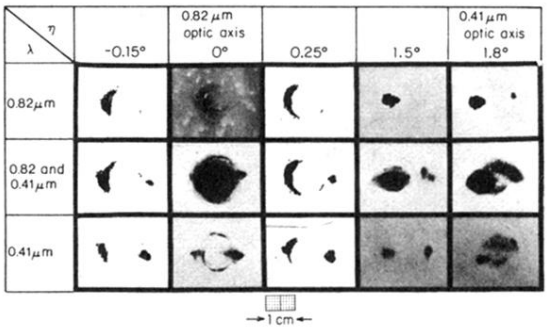

FIG. 10. Observed intensity patterns at the exit surface of a 2.4-cm thick crystal of α-iodic acid (magnification 8×). The angle between the light wave vectors and the optical axis at the fundamental wavelength (0.82 μm) is varied as indicated. The total power at the second harmonic is about one millionth of the fundamental power.

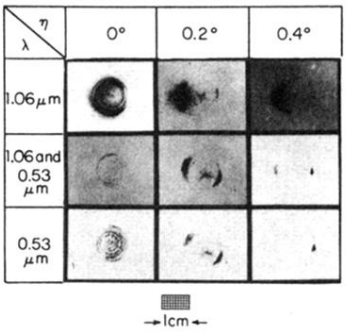

FIG. 11. Intensity patterns at 1.06 and 0.53 μm as a function of the angle between the wave normal and the fundamental optic axis. The SH optic axis is in nearly the same direction.